pp. 422-441

N63 20934
CODE NONE

Reprinted from ICARUS, Volume I, Number 5, 6, May 1963 p 422-441 15 refs
Copyright © 1963 by Academic Press Inc. *Printed in U.S.A.*

Reprint

ICARUS 1, 422-441 (1963)

The Early Evolution of the Sun

DILHAN EZER AND A. G. W. CAMERON

Goddard Institute for Space Studies, National Aeronautics and Space Administration, New York, N. Y.

ABST 20934

Received December 18, 1962

Hayashi has predicted that the early contracting sun should be highly luminous and fully convective, if one makes a correct choice of the photospheric boundary condition in constructing solar models in the contracting stages. We have constructed a sequence of models which fully confirm his predictions. The maximum radius of the protosun consistent with gravitational stability is $57\,R_\odot$; this has a luminosity of about 450 times that of the sun. As the protosun shrinks its stays fully convective until a radius of less than $3R_\odot$ is reached; the luminosity continues to decrease until a radius of $1.7R_\odot$ is reached. The sun requires about 2 million years to contract onto the main sequence, but this number is very uncertain because of the unsatisfactory state of convection theories. If the primitive solar material has the terrestrial ratio of deuterium to hydrogen, then a further 3×10^5 years is required to burn the deuterium. These numbers are very much less than previous studies had indicated. The degree of lithium burning in the outer convection zone of the sun is highly uncertain owing also to the unsatisfactory state of convection theories.

Introduction

The early contracting phase of solar evolution is of great interest to any theory of formation of the solar system (see for example Hoyle, 1960; Cameron, 1962*a*, 1962*b*). There is a tendency on the part of scientists attempting to reconstruct the history of the planets and meteorites to assume that the sun had its present properties, or at least that its luminosity was not greatly different from the present one, during the earliest history of the solar system. We shall see in the course of this work that such an assumption is questionable.

The first detailed study of an evolutionary sequence of contracting solar models was carried out by Henyey, Lelevier, and Levee (1955). This work indicated that the sun gradually increased in luminosity as it contracted. When nuclear energy generation sets in and halts the contraction near the main sequence, a moderate decline in luminosity takes place. The solar models of Henyey *et al.* did not make provision for the possibility of an outer convection zone.

A more recent study has been carried out by Brownlee and Cox (1961). These authors improved the calculations of Henyey *et al.* by using improved opacities for the solar interior, by incorporating an outer convection zone in the models, and by putting in all the sources of nuclear energy generation. However, they used only a crude surface boundary condition. The evolutionary paths followed by their models have a general resemblance to those of Henyey *et al.*

Recently Hayashi (1962) has pointed out that the surface boundary conditions in the more extended models of Henyey *et al.* and of Brownlee and Cox are not correct. The density of matter in the photospheric layers of such models is much too small. In the photosphere of the sun the opacity of the material must be such that the photospheric layer lies at about one optical depth in the solar atmosphere. Thus

CASE FILE COPY

Hayashi concluded that a readjustment of the contracting solar models would be necessary in which the density of the solar photospheric layer would be greatly increased.

Such a readjustment is possible only if there is a complete reorganization of the density-radius relation throughout the model. The models of Brownlee and Cox had rather shallow surface convection zones; an increase in surface density would require that the surface convection zone should extend much farther into the interior, possibly all the way to the center. Since convection is an exceedingly efficient mechanism of energy transport, the luminosity of the model would thus depend entirely upon the rate at which energy could be radiated away from the surface. Now, the opacity of solar material increases as the temperature increases, at least in the range 3×10^3 to 10^4 °K. Thus a high surface temperature also assists the model to attain a satisfactory photospheric boundary condition. However, it should be noted that this leads to the expectation that the solar luminosity was much higher than at present during the contraction phase.

The present work was undertaken to investigate these predictions of Hayashi. The results reported here are preliminary, in the sense that isolated solar models have been calculated rather than evolutionary sequences of models. No nuclear energy generation has been included, so that the luminosity derives entirely from the release of gravitational potential energy. It was necessary to make an assumption about the distribution of this energy source. All models were assumed to be in homologous contraction, so that the relative structure would not change in an infinitesimal contraction. With assumptions of this sort it is easier to explore the consequences of variations in interesting physical parameters entering into the models.

The Basic Equations of Stellar Structure

Stellar models are calculated on the assumption that the star is spherically symmetric and in hydrostatic equilibrium. The equations that must be satisfied by this structure are:

$$dM(r)/dr = 4\pi r^2 \rho \tag{1}$$

$$dP(r)/dr = -G[M(r)/r^2]\rho \tag{2}$$

$$dL(r)/dr = 4\pi r^2 \rho \epsilon \tag{3}$$

For radiative equilibrium:

$$\frac{dT}{dr} = -\frac{3\chi\rho}{4ac}\frac{1}{T^3}\frac{L(r)}{4\pi r^2} \tag{4a}$$

For convective equilibrium:

$$\frac{1}{T}\frac{dT}{dr} = \frac{\Gamma - 1}{\Gamma}\frac{1}{P}\frac{dP}{dr} \tag{4b}$$

In the above equations, P is the total pressure (gas plus radiation), T is the temperature, $M(r)$ is the mass within a sphere of radius r, $L(r)$ is energy crossing the surface of a sphere of radius r per second, ϵ is the energy produced per gram per second, χ is the absorption coefficient (cm^2/gm), and Γ is the effective ratio of the specific heats. It differs from $\gamma = c_p/c_v$ through the inclusion of the effects of dissociation and ionization of the gas, and it varies throughout the convection zone of the stars. The assumption Γ = constant = 5/3 corresponds to the assumption that the stellar material is wholly neutral or completely ionized.

Equations (1–4) are more easily integrated in electronic computers if they are expressed in logarithmic form. Neither the pressure nor the mass is very suitable to take as an independent variable all the way from surface to the center. Near the photosphere, where the change in pressure is rapid compared to the change in mass, and the energy transport by convection should be treated in the proper way, it is better to use pressure as an independent variable. Then Eqs. (1–4) can be written in logarithmic form with pressure as an independent variable:

$$\frac{d\ln r}{d\ln P} = \frac{d\mathbf{r}}{d\mathbf{P}} = -\exp(\mathbf{r} + \mathbf{P} - \ln G - \mathbf{M} - \varrho)$$

$$\frac{d\ln M}{d\ln P} = \frac{d\mathbf{M}}{d\mathbf{P}}$$

$$= -\exp\left(\ln\frac{4\pi}{G} + 4\mathbf{r} + \mathbf{P} - 2\mathbf{M}\right)$$

$$\frac{d\ln L}{d\ln P} = \frac{d\mathbf{L}}{d\mathbf{P}}$$

$$= -\exp\left(\ln\frac{4\pi}{G} + 4\mathbf{r} + \boldsymbol{\epsilon} + \mathbf{P} - \mathbf{M} - \mathbf{L}\right)$$

Radiative temperature gradient:

$$\frac{d\ln T}{d\ln P} = \frac{d\mathbf{T}}{d\mathbf{P}} = \nabla_{rad} = \exp\left(\ln\frac{3}{16\pi GaC} + \ln\chi + \mathbf{L} + \mathbf{P} - \mathbf{M} - 4\mathbf{T}\right)$$

The symbols indicate that $\mathbf{r} = \ln r$, $\mathbf{M} = \ln M$, etc. The temperature gradient in case of convection will be discussed later.

Even though the above equations can be used all the way from surface to the center, in cases where the change in mass becomes very large compared to the change in pressure, very small steps are needed. Then it is better to take mass as an independent variable. Our basic equations become:

$$d\mathbf{r}/d\mathbf{M} = \exp(\mathbf{M} - 3\mathbf{r} - \boldsymbol{\rho} - \ln 4\pi),$$

$$d\mathbf{P}/d\mathbf{M} = -\exp[\ln(6/4\pi) + 2\mathbf{M} - \mathbf{P} - 4\mathbf{r}],$$

$$d\mathbf{L}/d\mathbf{M} = \exp(\boldsymbol{\epsilon} + \mathbf{M} - \mathbf{L}),$$

and

$$d\mathbf{T}/d\mathbf{M} = -\exp[\ln(3/64ac\pi^2) + \mathbf{L} + \mathbf{M} - 4\mathbf{T} - 4\mathbf{r} + \ln\chi],$$

provided

$$\left|\frac{d\mathbf{T}}{d\mathbf{M}}\right| < \left|\frac{\Gamma - 1}{\Gamma}\frac{d\mathbf{P}}{d\mathbf{M}}\right|;$$

otherwise

$$\frac{d\mathbf{T}}{d\mathbf{M}} = \frac{\Gamma - 1}{\Gamma}\frac{d\mathbf{P}}{d\mathbf{M}}.$$

It should be noted that the second form for the equation of energy transport is needed where the radiative temperature gradient exceeds the adiabatic temperature gradient. Because the logarithmic mass is used as an independent variable only deep in the stellar interior, we make here the assumption that the full energy flux is carried by convection and that the temperature gradient is the adiabatic one. This assumption is good in the deep interior but fails badly near the stellar surface where the logarithmic pressure is used as an independent variable.

The Gravitational Energy Source

In this study of early solar evolution, the energy generation was assumed to be entirely due to release of the gravitational potential energy of the contracting solar mass.

The luminosity is

$$L = \int_0^R 4\pi r^2 \rho\epsilon(r)dr$$

where ϵ is energy released per gram of material per second due to contraction of the star.

$$\epsilon(r) = \frac{dL(r)}{4\pi r^2\rho dr}$$

If U indicates the internal energy per gram of material and V the specific volume, then at each point in the star

$$\frac{\partial U}{\partial t} = -\epsilon(r) - P\frac{\partial V}{\partial t}$$

The change of internal energy is balanced by the energy loss and the work done by the pressure. The internal energy per gram of material at a point inside the star is

$$U = c_v T(r)$$

Assuming the ideal gas law governs the interior of the star,

$$U = \frac{1}{(\Gamma - 1)}\frac{P(r)}{\rho(r)},$$

where Γ is the ratio of specific heats at the point considered. If we replace V by its reciprocal ρ, then:

$$-\epsilon(r) = \frac{1}{(\Gamma - 1)}\frac{\partial}{\partial t}\left(\frac{P}{\rho}\right) + P\frac{\partial}{\partial t}\left(\frac{1}{\rho}\right),$$

or

$$-\epsilon(r) = \frac{1}{(\Gamma - 1)}\frac{1}{\rho}\frac{\partial P}{\partial t} - \frac{\Gamma}{(\Gamma - 1)}\frac{P}{\rho^2}\frac{\partial\rho}{\partial t}. \quad (5)$$

If it is assumed that the star is contracting homologously, then the rate of change

with time of pressure and density at every point is completely determined by the rate of change in the radius of the star in such a way that

$$\frac{1}{4P}\frac{\partial P}{\partial t} = -\frac{1}{R}\frac{dR}{dt} \quad \text{and} \quad \frac{1}{3\rho}\frac{\partial \rho}{\partial t} = -\frac{1}{R}\frac{dR}{dt}$$

Inserting these values in Eq. (5):

$$\epsilon(r) = \frac{3\Gamma - 4}{\Gamma - 1}\frac{P(r)}{\rho(r)}\left(-\frac{1}{R}\frac{dR}{dt}\right).$$

Hence

$$L = 4\pi\left(-\frac{1}{R}\frac{dR}{dt}\right)\int_0^R \left(\frac{3\Gamma - 4}{\Gamma - 1}\right) P(r)r^2dr.$$

The rate of contraction may be written

$$-\frac{1}{R}\frac{dR}{dt} = \frac{L}{4\pi\int_0^R [(3\Gamma - 4)/(\Gamma - 1)]\, P(r)r^2dr} = J\frac{LR}{GM^2}.$$

It may thus be seen that we are expressing the reciprocal time for the contraction rate as a fraction of the ratio of the luminosity to a measure of the gravitational potential energy. The quantity J may be called the contraction parameter; it is one of the fundamental parameters that had to be adjusted in order to obtain consistent solar models. It is by definition

$$J = \frac{GM^2}{4\pi R\int_0^R [(3\Gamma - 4)/(\Gamma - 1)]P(r)r^2dr}$$

It may easily be seen that the contraction parameter should not vary rapidly from one solar model to a later one. If the sun were a polytrope of index n with a constant ratio of specific heats throughout, then we would have

$$J = \frac{(\gamma - 1)(5 - n)}{3\gamma - 4}.$$

Opacities

The computer programming code for stellar absorption coefficients and opacities (Cox, 1961), which was prepared at the Los Alamos Scientific Laboratory, was kindly made available for the present opacity calculations. The program was run on an IBM 7090 at the Institute for Space Studies for a temperature range of 2×10^3 °K through 5×10^7 °K and a density range of 10^{-12} through 10^3 gm/cm^3, with a mixture containing hydrogen, helium, and heavy elements having mass fractions 0.602, 0.376, and 0.022, respectively. The code requires use of the abundance of each element separately.

The code could be run for a mixture of not more than 11 elements. A modified version of an abundance table (Cameron, 1959) was adopted and the individual elements were combined to give the representative abundances shown in Table I. The rather rare element K was retained because of its importance in supplying electrons for the formation of H^- at low temperatures.

The processes which contribute to the opacity calculation in the code are bound–bound absorption, bound–free absorption, free–free absorption, electron scattering, negative ion absorption, and electron conduction.

The bound–bound absorption by many lines close together (blanketing) has been important in stellar atmospheres and interiors. Its influence on the opacity depends on the position of the line in the emission spectrum and, to a lesser degree, the shape of the line. In stellar atmospheres Stark broadening of hydrogen lines is dominant,

TABLE I

Adopted Abundances of Elements (Silicon = 10^6)

Element	Abundance	Element	Abundance	Element	Abundance
H	3.2×10^{10}	O	2.9044×10^7	K	3.3×10^3
He	5.0×10^9	Ne	1.7×10^7	Ca	1.99×10^5
C	1.66×10^7	Al	9.5×10^4	Fe	2.629×10^5
N	3.0×10^6	Si	2.303×10^6		

but in the deep interiors of the star collisional broadening is the most important below 10^6 °K; lines can increase the opacity by a factor of two or more. At the temperatures prevailing in the interiors of stars, the increase is about 10% of the total opacity.

The bound–free absorption depends on the equilibrium number of electrons which are bound in the various atomic states. When the ionization of one element is completed, no more bound–free absorption due to that element can occur. In the mixture under consideration, the bound–free absorption by the K shell electrons of iron keeps the opacity moderately large up to several million degrees.

At temperatures around 10^7 °K, most elements in astrophysical mixtures have been ionized, and free–free absorption in the field of hydrogen ions becomes very important. The nuclear charge is shielded by free electrons and ions resulting in a decrease in the free–free absorption. But these effects are about 10% or less at moderate densities and temperatures around 10^6 °K. When electrons are degenerate, electron conduction also contributes to the transport of energy. But these cases are not important in the temperature and density ranges we are interested in.

The only negative ion of importance in astrophysics is that of hydrogen. At the low temperatures such as occur at the outer layer of stars, H^- ions formed from the capture of electrons from the metals keep the opacity still quite high. Both H^- bound–free and free–free absorptions contribute to the opacity. Actually H^- free–free absorption, which depends on the number of free electrons, is only important at wavelengths near or longer than the H^- bound–free edge.

Molecular absorption and Rayleigh

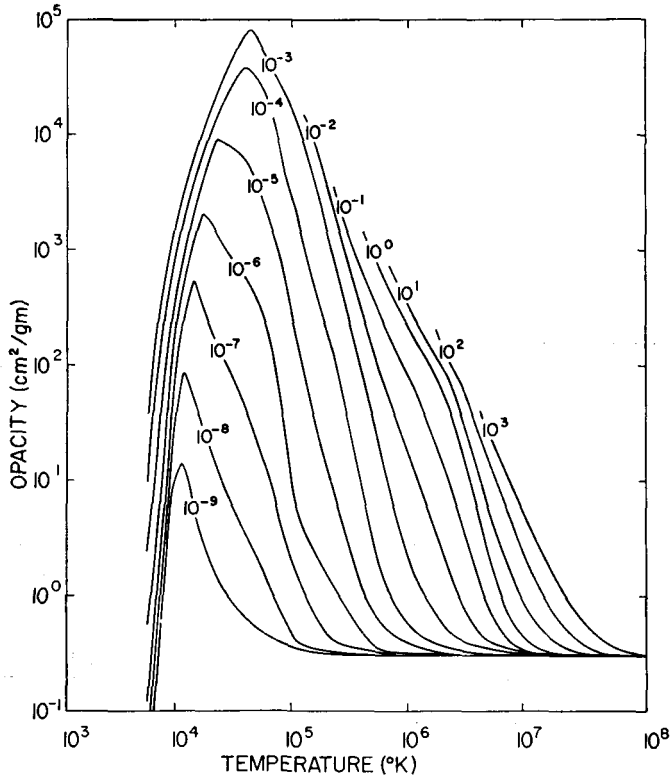

FIG. 1. Opacities for lines of indicated density (gm/cm³) calculated as a function of temperature from the Los Alamos Opacity Code.

scattering have not been included in the opacity calculation. Unfortunately very little is known about the absorption due to molecules that form in stellar atmospheres. Blanketing effects due to overlapping molecular bands should be very important at these low temperatures. Therefore, the opacities at low temperatures are very uncertain. Rayleigh scattering, which is included in Vitense's opacity calculations (Bohm-Vitense, 1951), is usually not very important. Only at very low temperatures and for low metal contents might it become important.

The calculated opacities require corrections due to the absorption by lines. A. N. Cox gives these corrections as a graph (private communication) and the application of these corrections increases the opacities by a factor of 1.1 to about 3.0 depending on the density and temperature combination.

Figure 1 shows the over-all run of opacities calculated for different densities as a function of temperature. Figure 2 shows in more detail the opacities at low temperatures.

These opacities have been stored in the machine as a two-dimensional table corresponding to discrete values of ln T and ln ρ. For a given ln T and ln ρ combination the corresponding opacity (ln χ) was obtained by linear interpolation.

Equation of State

The total pressure is given by the sum of gas pressure plus radiation pressure,

$$P = P_g + P_r,$$
$$P_g = (1 + \bar{x})(NkT/V)$$
$$P_r = \tfrac{1}{3}aT^3$$

where N is the number of atoms per unit volume, V is the specific volume, and a is the radiation constant; $\bar{x}$ is the mean degree ionization and dissociation defined by

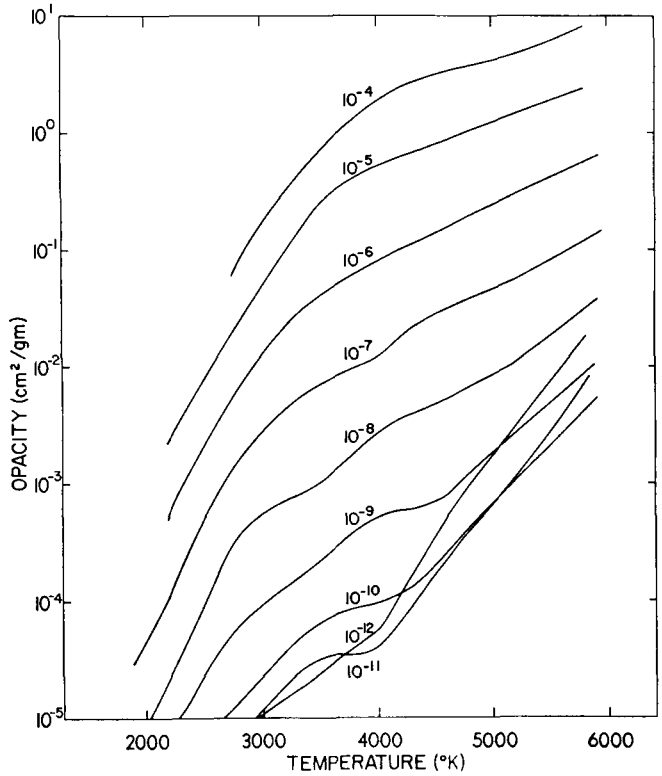

Fig. 2. Details of the opacities at low temperatures. The lines refer to the indicated densities.

$$\bar{x} = \Sigma \nu_i \eta_i - (x_4/2)\nu_1$$

where η_i are the degrees of ionization, x_4 is the fraction of hydrogen nuclei in molecular state, and ν_i are the abundances by number of various elements under consideration, with $\Sigma\ \nu_i = 1$. The partial electron pressure P_E and the partial pressure of atomic hydrogen P_H are given by

$$P_E = \frac{\bar{x} P_g}{1 + \bar{x}} \qquad P_H = \frac{[1 + \eta_1 - (x_4/2)]\nu_1 P_g}{1 + \bar{x}}$$

The density ρ is related to P and T through the equation of state

$$P_g = (\Re/\mu)\rho T;$$

with the above definition for the mean molecular weight μ we have

$$\mu = \frac{\mu_0}{1 + \bar{x}}$$

with $\mu_0 = 4/(4X + Y)$, where X and Y are the mass fractions of hydrogen and helium, respectively.

As a chemical composition we use 0.602 for the mass fraction of hydrogen, 0.376 for helium, and 0.022 for the heavy elements. Hydrogen and helium have each been considered in three states: H_2, H, H^+ and He, He^+, He^{2+}. The dissociation equilibrium constant for molecular hydrogen is given by a polynomial of θ $(= 5040/T)$ which is used in the calculations of Vardya (1961).

$$\log_{10} K(H_2) = \log \frac{P^2_H}{P_{H_2}} = 12.533505 - 4.9251644\ \theta + 0.056191273\ \theta^2 - 0.0032687661\ \theta^3$$

Here P_H denotes the partial pressure of atomic hydrogen, and P_{H^2} that of molecular hydrogen. The amount of molecular hydrogen is only calculated in the temperature range 1000 °K to 12000 °K.

The degree of ionization for each element is obtained from the Saha equation;

$$\frac{\eta_i}{1 - \eta_i} \frac{\bar{x}}{1 + \bar{x}} P_g = \text{Const}\ T^{5/2} e^{\chi_i/kT}$$

where χ_i is the ionization potential and k is the Boltzman constant. At each integration step the program computes the degree of ionization and dissociation.

Convection

The existence of an outer convection zone greatly affects the luminosity and radius of late type stars. These two quantities are the boundary conditions for the interior models of the stars. Therefore, convection should be treated as accurately as possible. We use Prandtl's mixing length theory as applied by E. Bohm-Vitense (1958).

In the ionization zone where the absorption coefficient increases rapidly and the adiabatic gradient decreases with increasing temperature, the temperature gradient $\nabla = d \ln T/d \ln P$ becomes very steep and the local adiabatic gradient ∇_{ad} falls below it. Consequently the gas will become unstable against convection. A temperature gradient will be set up in such a way that the total flux will be carried partly by radiation and partly by convection. Moreover, when convective instability occurs, the turbulent elements do not move strictly adiabatically. The rising and falling turbulent elements and their surroundings exchange heat; the temperatures of the elements differ from their surrounding material. If ∇' $(= d \ln T'/d \ln P)$ shows the logarithmic temperature gradient of a moving turbulent element, then the main equations for the convective theory can be summarized as follows:

When the instability criterion

$$\nabla_{ad} < \nabla$$

is satisfied, we have

$$F_{rad} + F_{con} = F_{total} = L/4\pi R^2. \qquad (6)$$

The radiative flux is given by

$$F_{rad} = \frac{16\sigma T^4}{3\ \chi\ \rho H} \nabla. \qquad (7)$$

The convective flux is given by

$$F_{conv} = c_p \rho T \bar{v} (l/2H)(\nabla - \nabla'). \qquad (8)$$

Here, c_p is the specific heat per gram at constant pressure, $\bar{v}$ is the mean velocity of the rising or falling turbulent elements, $H = \Re T/\beta\mu g$ is the pressure scale height, and l is the mixing length, a distance which a moving element travels before disappearing into the surroundings. For most of this work we have assumed $l = H$. Also

g is the gravitational acceleration and β is the ratio of the gas pressure to total pressure. The mean velocity is

$$\bar{v} = (l/2)\sqrt{(g/H)C}(\nabla - \nabla')^{1/2}. \quad (9)$$

Here C takes care of the change of the degree of ionization of matter with temperature and density changes and can be expressed by

$$C = 1 - \frac{\partial \ln \mu}{\partial \ln T}.$$

The temperature of a moving element is given by a relation which represents the ratio of the excess energy content of the element to its radiation during its lifetime.

$$\frac{\nabla' - \nabla}{\nabla_{ad} - \nabla'} = c_p \rho T \frac{\chi \rho l}{24\sigma T^4}\bar{v} \quad (10)$$

The adiabatic temperature gradient for a material which is undergoing dissociation or ionization can be obtained from the entropy condition. The total internal energy of the volume V which contains matter and radiation is the sum of the kinetic and potential energies of the particles and the radiation energy of the volume:

$$U = [\tfrac{3}{2}(1 + \bar{x})kT + \Sigma \nu_i \eta_i \chi_i]N + VaT^4.$$

For an adiabatic change,

$$dU + PdV = 0.$$

The above two equations, together with equation of state and the Saha equation for the ionization, make it possible to give a general expression for the adiabatic gradient in terms of known quantities

$$\nabla_{ad} = \left(\frac{d \ln T}{d \ln P}\right)_{ad} = \frac{F_1}{F_2}$$

$$F_1 = (1 + \bar{x}) + \frac{f_1}{f_2}\sum \nu_i \eta_i (1 - \eta_i)\left(\frac{5}{2} + \frac{\chi_i}{kT}\right) + 4\frac{(1 - \beta)}{\beta}\left[(1 + \bar{x}) + \frac{f_1}{f_2}\sum \nu_i \eta_i (1 - \eta_i)\right]$$

$$F_2 = \frac{5}{2}(1 + \bar{x}) + \sum \nu_i \eta_i (1 - \eta_i)\left(\frac{5}{2} + \frac{\chi_i}{kT}\right)^2 - \frac{[\Sigma \nu_i \eta_i (1 - \eta_i)(\frac{5}{2} + \chi_i/kT)]^2}{f_2} + 4\frac{(1 - \beta)}{\beta}\left[4(1 + \bar{x}) + \frac{f_1}{f_2}\sum \nu_i \eta_i (1 - \eta_i)\left(\frac{5}{2} + \frac{\chi_i}{kT}\right)\right]$$

where $f_1 = \bar{x} + \bar{x}^2$ and $f_2 = 2\bar{x} + \bar{x}^2 - \Sigma \nu_i \eta_i^2$. They are taken as equal to $1 + \bar{x}$ and $1 + \bar{x} - (\Sigma \nu_i \eta_i / \mu_0)$ in the case of dissociation of hydrogen molecules under consideration. In this expression the variation with temperature of the molecular hydrogen partition function was neglected because of the small abundances of this molecule present in any of the models calculated in this paper. Should this assumption not be warranted, then one should use the thermodynamic functions given by Vardya (1961). The specific heat c_p, which is the partial derivative of U with respect to T, may be written as

$$c_p = (\Re/\mu_0)F_2.$$

The Eqs. (6), (7), (8), (9), and (10) are the main equations which will give us the real temperature–pressure relation in the layers where convection sets in. These five equations determine the actual logarithmic temperature gradient ∇, the logarithmic temperature gradient of the turbulent element ∇'. the velocity of the moving turbulent elements, the amount of flux carried by radiation F_{rad}, and that carried by convection F_{conv}, satisfying the condition that $F_{rad} + F_{conv}$ is equal to total flux. The convection will set in when $\nabla > \nabla_{ad}$. Since the radiative temperature gradient is the largest value that the actual temperature gradient can take, then ∇ must be between ∇_{rad} and ∇_{ad}. It is close to ∇_{rad} if the greater part of the energy is carried by radiation. and it has a value slightly above ∇_{ad} if most of the energy is carried by convection. On the other hand, if during the convection, the moving elements lost no energy, then the temperature gradient of the turbulent elements ∇' would be equal to ∇_{ad}. The moving elements never possess a temperature gradient steeper than the surrounding temperature gradient, since a rising element radiates energy to its neighborhood. Consequently the four tempera-

ture gradients should always maintain the relative order

$$\nabla_{rad} > \nabla > \nabla' > \nabla_{ad}.$$

We use the following procedure in order to obtain the actual temperature gradient. Once T and P are known at a point, a subroutine calculates the degree of ionization, the mean molecular weight, the adiabatic gradient, the specific heat c_p, and C. The Eqs. (6), (7), (8), (9), and (10) can be written in the following form:

$$w\nabla + Q(\nabla - \nabla')^{3/2} = F \tag{6'}$$

$$F_{rad} = w\nabla \tag{7'}$$

$$F_{conv} = Q(\nabla - \nabla')^{3/2} \tag{8'}$$

$$\bar{v} = q_1(\nabla - \nabla')^{1/2} \tag{9'}$$

$$(\nabla' - \nabla_{ad}) = (9/4)(w/Q)(\nabla - \nabla')^{1/2} \tag{10'}$$

where

$$w = \frac{16\sigma T^4}{3\chi\rho H}, \qquad q_1 = \frac{l}{2}\sqrt{\frac{g}{H}}\,C,$$

$$q_2 = c_p\rho T\frac{l}{2H}, \qquad Q = q_1q_2.$$

These equations can be combined to give a cubic equation

$$\frac{Q}{w}\Delta\nabla^3 + \Delta\nabla^2 + \frac{9}{4}\frac{w}{Q}\Delta\nabla + \left(\nabla_{ad} - \frac{F}{w}\right) = 0 \tag{11}$$

in terms of $\Delta\nabla$, where $\Delta\nabla = (\nabla - \nabla')^{1/2}$.

If the radiative gradient becomes larger than the adiabatic gradient, the cubic equation is solved for $\Delta\nabla$ by Newton's method. Then Eqs. (9') and (10') give us $\bar{v}$ and ∇'. F_{rad} and F_{conv} are obtained with Eq. (7') and (8'). We can check whether the condition (6) is satisfied. If it is not satisfactory, the values can be improved by iteration.

At great depths, the elements move almost adiabatically, and the actual temperature gradient approaches the adiabatic gradient. Convection is so efficient in transporting energy that we may use the convective temperature gradient as defined

$$\frac{d\mathbf{T}}{d\mathbf{m}} = \frac{\Gamma - 1}{\Gamma}\frac{d\mathbf{P}}{d\mathbf{m}}$$

provided that the actual values of Γ corresponding to the physical conditions existing at every point in the zone are taken into account.

Atmospheric Calculations

For an assumed mass, radius, and expected luminosity of the configuration, the effective temperature of the star,

$$T_{eff} = \frac{L}{4\pi R^2\sigma}$$

is calculated. For the photospheric pressure:

$$\frac{dP_{ph}}{d\tau} = \frac{g}{\chi}$$

where $g = GM/R^2$, χ is the absorption coefficient per gram of stellar material, and τ is the optical depth.

We start the calculations with an assumed photospheric density ρ_{ph}, and $\chi(\rho_{ph}, T_e)$ gives us the corresponding photospheric pressure at a chosen optical depth. Now the degree of ionization and dissociation allows us to define the mean molecular weight. From the equation of state:

$$P = (\mathcal{R}/\mu)\rho T$$

a new ρ is determined. This procedure is repeated until P_{ph}, ρ_{ph}, T_e, $\chi(\rho_{ph}, T_e)$, and τ are adjusted at a selected optical depth. From the study of the radiative transfer in stellar atmospheres, it is found that the effective temperature of the stars approximately corresponds to the temperature at the optical depth $\tau = 2/3$. We therefore used $\tau = 2/3$ in the calculation of our stellar models. In order to see the influence of different values of τ, we repeated the calculation for some models using $\tau = 1$ and $\tau = 0.5$. Due to the present uncertainties in the opacity at low temperatures, no attempt has been made to improve these crude atmospheric calculations.

Integration Procedure

To get the final model for a star of fixed mass and radius, a computing program, using logarithmic variables, has been prepared for the 7090 computer which carries

out the integrations and fitting procedure entirely automatically. With a fixed mass, radius, and trial luminosity of the star, atmospheric conditions provide us the boundary values for inward integrations. The luminosity L and the contraction rate J are the eigenvalues for these inward integrations. The final model cannot be obtained unless we have the right combination of L and J values which suits the internal structure of the star.

Integration starts from the surface using $\ln P$ as the independent variable. As a step size $\Delta \ln P = 0.1$ is stored in the machine, but the interval is halved or doubled according to the size of the derivatives. When the radiative temperature gradient gets larger than the simultaneously calculated adiabatic gradient, the actual temperature gradient is obtained as explained above. When $d\mathbf{M}/d\mathbf{P}$ is larger than a preassigned value, the program switches to the second set of equations in which the mass is used as an independent variable. Special care is taken in order to keep a uniform change in mass and pressure at the switchover point.

Preliminary trial inward integrations are carried out until the solutions reach within about 1% of the mass at the center. Stability of the integration is checked in terms of homology invariants

$$U = \frac{d \ln M}{d \ln r}; \qquad W = \frac{d \ln L}{d \ln r}$$

which both should approach 3 near the center of the star. If the U value stays smaller than 3, the trial luminosity should be decreased; if it stays larger than 3 as the center is approached the trial luminosity should be increased. The systematic character of the W curve is also found to be a function of the trial eigenvalue of J. If W becomes smaller near the center, J should be increased; however, if it passes 3, the value should be decreased. Figure 3 schematically illustrates the character of these (U, W) curves as functions of the trial eigenvalues. The center sketch shows the behavior of the (U, W) curves with the right combination of eigenvalues L and J. The other figures illustrate the misbehavior of the curves with too large or too small combinations of the trial eigenvalues. The program automatically checks U and W values and gives better trial values according to the mass point where the mis-

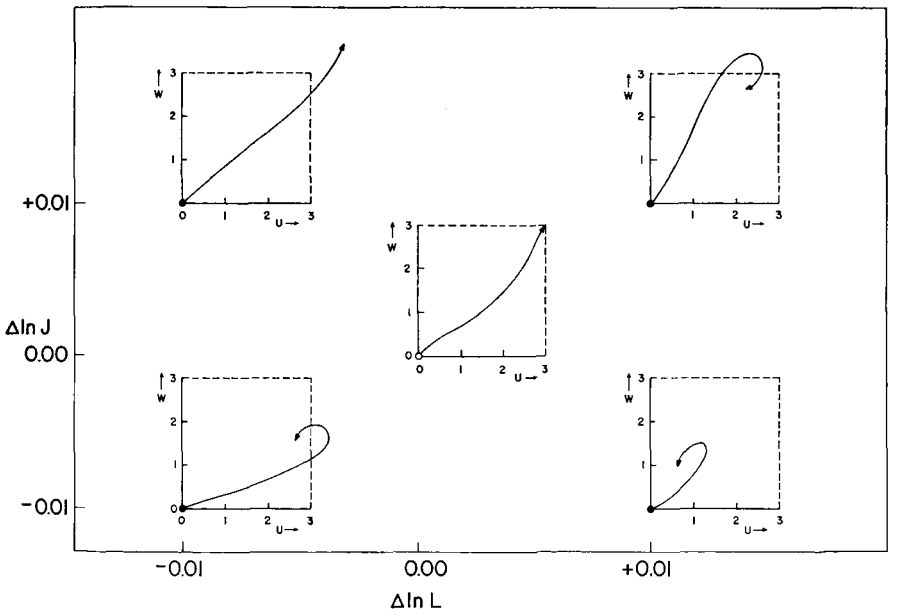

FIG. 3. Diagrams showing the behavior of the homologous variables U and W as a function of the assumed surface eigenvalues of the model, centered about the correct choice of these eigenvalues.

behavior starts and defines an upper and lower limit for each one as long as the other is behaving properly. The U value, which is the ratio of the local density to the mean density, needs special care in the ionization zones of hydrogen and helium. In these zones the local density might decrease with increasing geometrical depth, and our criteria for checking the stability of integrations by means of U might misdirect us; care is taken to avoid such misdirection.

The program tries to adjust the L and J values until the integrations are carried out to within 1% of the central mass. The program then obtains the trial center values for pressure P_c and temperature T_c by extrapolating from the values where the properly behaving inward integrations stop. The outward integration starts by series expansion at the mass $M_0 = e^{-8} M$, where M is the total mass of the star, and is carried out up to the preassigned fitting point. The selection of right L and J values is very important since they affect the starting values of the outward integrations through the energy generation equation. If the trial eigenvalues of the integrations are far from the real conditions that the star should have, the fitting procedure is never achieved.

The fitting procedure is accomplished in the following manner: Two other inward integrations with small increments in L or J are performed, thus providing three inward integrations with the eigenvalues.

$$\begin{array}{ll} L, & J \\ L, & J + \delta J \\ L + \delta L, & J \end{array}$$

The comparison of these integrations at the preassigned fitting point gives the dependence of each dependent physical variables on the eigenvalues:

$$\frac{\delta Y_{i_{in}}}{\delta L}, \qquad \frac{\delta Y_{i_{in}}}{\delta J}$$

where Y_i $(i = 1, \ldots, 4)$ are ln L, ln R, ln P, and ln T, respectively.

A similar set of four outward integrations, from the center to the fitting point are performed, with the trial eigenvalues

$$\begin{array}{llll} P_c + \delta P_c, & T_c, & L, & J \\ P_c, & T_c + \delta T_c, & L, & J \\ P_c, & T_c, & L + \delta L, & J \\ P_c, & T_c, & L, & J + \delta J. \end{array}$$

The results are compared with the outward integration of the eigenvalues P_c, T_c, L, J, in order to obtain the eigenvalue dependence

$$\frac{\delta Y_{i_{out}}}{\delta P_c}, \qquad \frac{\delta Y_{i_{out}}}{\delta T_c}, \qquad \frac{\delta Y_{i_{out}}}{\delta L}, \qquad \frac{\delta Y_{i_{out}}}{\delta J}$$

of the physical variables at the fitting point.

The corrections ΔP_c, ΔT_c, ΔL, ΔJ to the trial eigenvalues of P_c, T_c, L, and J, which will give us smaller differences at the fitting point, can be obtained by solving four simultaneous linear equations,

$$\begin{aligned} \Delta D_i = {} & \frac{\delta Y_{i_{out}}}{\delta P_c} \Delta P_c + \frac{\delta Y_{i_{out}}}{\delta T_c} \Delta T_c \\ & + \left(\frac{\delta Y_{i_{out}}}{\delta L} - \frac{\delta Y_{i_{in}}}{\delta L} \right) \Delta L \\ & + \left(\frac{\delta Y_{i_{out}}}{\delta J} - \frac{\delta Y_{i_{in}}}{\delta J} \right) \Delta J \end{aligned}$$

where ΔD_i $(i = 1, \ldots, 4)$ are the differences at the fitting point between inward and outward integrations in physical variables. The procedure is repeated using better trial values, until the differences at the fitting point become smaller than a desired value.

Results

Twenty-seven models for the early contracting sun, each corresponding to a radius expressed as a multiple of the present solar radius, have been constructed. The results of the computations have been summarized in Table II for fully convective models and in Table III for partially convective models. Each column shows, in turn, the radius in terms of solar radius, the luminosity in terms of solar luminosity, the effective temperature of the model, the contraction parameter, the central temperature of the model, the center and surface densities, and the ratio of the central density to the mean density of the model.

TABLE II
CHARACTERISTICS OF FULLY CONVECTIVE MODELS

$R/R\odot$	$L/L\odot$	T_e (°K)	J	T_{center} (°K)	ρ_{center} (gm/cm³)	$\rho_{surface}$ (gm/cm³)	$\rho_c/\bar{\rho}$
3	3.470	4535	2.107	2.923×10^6	3.721×10^{-1}	1.829×10^{-7}	7.12
5	8.790	4432	2.080	1.779×10^6	8.301×10^{-2}	1.098×10^{-7}	7.35
10	28.677	4212	2.041	9.148×10^5	1.228×10^{-2}	6.197×10^{-8}	8.70
20	88.910	3941	2.015	4.758×10^5	1.606×10^{-3}	3.638×10^{-8}	9.10
25	124.68	3847	2.020	3.870×10^5	8.794×10^{-4}	3.089×10^{-8}	9.74
30	165.30	3768	2.062	3.269×10^5	5.377×10^{-4}	2.722×10^{-8}	10.3
50	343.91	3505	2.607	1.902×10^5	1.102×10^{-4}	2.048×10^{-8}	9.76
55	414.50	3502	2.436	1.848×10^5	1.059×10^{-4}	1.855×10^{-8}	12.48
60	475.13	3469	2.824	1.622×10^5	7.194×10^{-5}	1.782×10^{-8}	11.02
75	651.82	3358	3.024	1.389×10^5	4.932×10^{-5}	1.558×10^{-8}	14.74
100	976.72	3218	3.699	9.609×10^4	1.872×10^{-5}	1.313×10^{-8}	13.27
200	2555.0	2894	3.156	4.723×10^4	1.637×10^{-6}	8.595×10^{-9}	9.28
400	7325.4	2663	2.785	1.990×10^4	1.341×10^{-7}	7.374×10^{-9}	6.08
450	8107.9	2575	2.486	1.722×10^4	6.905×10^{-8}	8.464×10^{-9}	4.20
500	10730	2621	2.604	1.556×10^4	3.964×10^{-8}	6.444×10^{-9}	2.84
600	16078	2646	3.329	1.348×10^4	1.448×10^{-8}	4.798×10^{-9}	0.53
750	27900	2716	3.165	1.166×10^4	3.875×10^{-9}	2.997×10^{-9}	0.27
1000	62160	2874	0.595	1.101×10^4	1.027×10^{-9}	1.445×10^{-9}	0.73

TABLE III
CHARACTERISTICS OF PARTIALLY CONVECTIVE MODELS

$R/R\odot$	$L/L\odot$	T_e (°K)	J	T_{center} (°K)	ρ_{center} (gm/cm³)	$\rho_{surface}$ (gm/cm³)	$\rho_c/\bar{\rho}$
1.00	4.06	8169	0.748	2.270×10^7	479	1.293×10^{-8}	339
1.20	3.73	7306	0.779	1.888×10^7	263	3.035×10^{-8}	322
1.50	1.70	5374	1.234	9.622×10^6	41.62	2.171×10^{-7}	99.5
1.60	1.09	4658	2.096	5.220×10^6	4.644	3.456×10^{-7}	13.4
1.75	1.15	4507	2.080	4.574×10^6	2.210	3.545×10^{-7}	8.39
1.85	1.32	4538	2.088	4.453×10^6	1.796	3.228×10^{-7}	8.06
2.00	1.56	4550	2.120	4.206×10^6	1.302	2.915×10^{-7}	7.39
2.25	1.98	4551	2.110	3.848×10^6	0.884	2.533×10^{-7}	7.13
2.50	2.44	4548	2.095	3.512×10^6	0.647	2.242×10^{-7}	7.16

For all models above 2.5 solar radii, the convection is complete all the way to the center. When the sun contracts to a radius smaller than three solar radii, the radiative core starts to develop. Additional characteristics for these models are indicated in Table IV; the second and third columns give the temperature and density at the bottom of the convection zone, the fourth column the mass fraction inside the radiative core which increases with decreasing radius; and the fifth column is the fraction of the radius covered by the radiative core.

In Table V, we show the gravitational

TABLE IV
SOME PHYSICAL CHARACTERISTICS AT BASE OF CONVECTION ZONES

$R/R\odot$	T (°K)	ρ	(M_r/M)	(r/R)
1.00	6.68×10^4	2.66×10^{-8}	1.00	1.00
1.20	7.10×10^4	5.08×10^{-7}	.99	.99
1.50	1.46×10^5	7.50×10^{-2}	.97	.70
1.60	2.58×10^6	7.68×10^{-1}	.60	.51
1.75	3.00×10^6	1.15	.52	.44
1.85	3.29×10^6	0.96	.40	.40
2.00	3.31×10^6	0.94	.15	.33
2.25	3.35×10^6	0.78	.08	.17
2.50	3.38×10^6	0.64	.002	.05

TABLE V

DETAILS OF INTERNAL ENERGIES AND STATES OF IONIZATION

$R/R_\odot$	E_{grav}	$E_{thermal}$	$E_{ionization}$	$X(H_2)$	$X(H)$	$X(H^+)$	$Y(He)$	$Y(He^+)$	$Y(He^{2+})$
1	9.941×10^{48}	5.150×10^{48}	2.957×10^{46}	—	neg	0.602	neg	neg	0.376
2	1.714×10^{47}	8.636×10^{47}	2.941×10^{46}	—	0.002	.600	neg	0.003	.373
2.25	1.527×10^{48}	7.653×10^{47}	2.938×10^{46}	—	.002	.600	neg	.003	.373
2.5	1.318×10^{48}	6.545×10^{47}	2.938×10^{46}	—	.002	.600	neg	.004	.372
3.0	1.150×10^{48}	5.772×10^{47}	2.936×10^{46}	—	.002	.600	neg	.004	.372
5	6.991×10^{47}	3.529×10^{47}	2.932×10^{46}	—	.002	.600	neg	.006	.370
10	3.492×10^{47}	1.799×10^{47}	2.818×10^{46}	—	.002	.600	neg	.014	.362
20	1.868×10^{47}	9.723×10^{46}	2.874×10^{46}	—	.002	.600	neg	.029	.347
25	1.522×10^{47}	8.024×10^{46}	2.842×10^{46}	—	.002	.600	neg	.042	.334
30	1.287×10^{47}	6.926×10^{46}	2.809×10^{46}	—	.002	.600	0.001	.053	.322
50	7.501×10^{46}	4.738×10^{46}	2.669×10^{46}	—	.002	.600	.004	.107	.265
55	7.311×10^{46}	4.611×10^{46}	2.631×10^{46}	—	.002	.600	.006	.111	.259
60	6.426×10^{46}	4.298×10^{46}	2.583×10^{46}	—	.002	.600	.008	.131	.237
75	5.550×10^{46}	3.9601×10^{46}	2.477×10^{46}	—	.003	.599	.018	.155	.203
100	3.940×10^{46}	3.454×10^{46}	2.263×10^{46}	—	.003	.599	.027	.227	.122
200	1.788×10^{46}	1.450×10^{46}	1.718×10^{46}	1.6×10^{-5}	.037	.565	.153	.222	.001
400	7.487×10^{45}	1.062×10^{46}	1.067×10^{46}	3.2×10^{-4}	.191	.411	.368	.008	neg
450	6.244×10^{45}	9.581×10^{45}	9.394×10^{45}	5.1×10^{-4}	.240	.362	.375	.001	neg
500	5.375×10^{45}	8.063×10^{45}	8.161×10^{45}	6.5×10^{-4}	.238	.364	.376	neg	neg
600	4.138×10^{45}	5.657×10^{45}	6.364×10^{45}	1.3×10^{-3}	.3542	.247	.376	neg	neg
750	2.892×10^{45}	4.088×10^{45}	5.193×10^{45}	4.4×10^{-3}	.4005	.2018	.376	neg	neg
1000	2.188×10^{45}	8.181×10^{45}	3.108×10^{45}	6.8×10^{-3}	.476	.119	.376	neg	neg

potential energy, the thermal energy, and ionization and dissociation energy, in ergs, for the indicated models. Meanwhile, the fractional mass in the form of molecules, neutral and ionized hydrogen, and neutral, singly, and doubly ionized helium are given. For the models $R/R_\odot > 57$, the absolute value of the gravitational potential energy is less than the sum of the thermal, ionization, and dissociation energies of the material.

These models are in the region of instability against gravitational collapse (Cameron, 1962*a*). Hence, they are only of formal interest. The collapse of the protosun continues until the hydrogen is fully ionized, 32% of helium is singly ionized, and 66% of helium is doubly ionized. This corresponds to a radius of 57 $R_\odot$, at which point gravitational stability sets in. The further contraction of the protosun occurs on the Kelvin-Helmholtz time scale.

In Fig. 4, the position of the models in the Hertzsprung-Russell diagram is shown. The threshold for stability corresponds to $R = 57\,R_\odot$. The luminosity of the protosun, corresponding to this radius, is about 450 $L_\odot$. For all models above 2.5 solar radii, the convection is complete all the way to the center. When the protosun contracts to 3 solar radii, its central temperature reaches about 2.9×10^6 °K and the

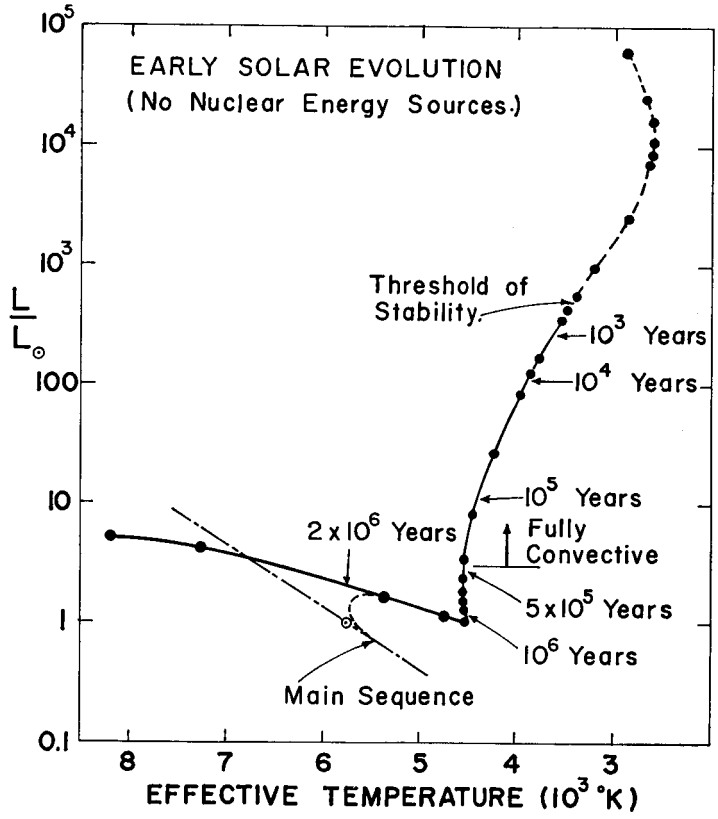

FIG. 4. The Hertzsprung-Russell diagram for the models of the contracting sun calculated in this paper, with the mixing length equal to the pressure scale height. Above the indicated threshold of stability the models are of academic interest only since the thermal, ionization, and dissociation energies exceed the magnitude of the gravitational potential energy. The models are fully convective above the line of evolution away from the threshold of stability as indicated at various points along the track. The main sequence and the present position of the sun are indicated by the dash-dot line on the lower left and by the circle. The sun probably approaches the main sequence approximately along the dashed line shown beyond the third last calculated model.

luminosity is about 3.47 times solar luminosity. With further contraction a radiative core starts to develop at the center. When the sun contracts to 2 solar radii, the radiative core covers about 15% of the mass and 33% of the radius. The luminosity reaches its minimum value when the radius becomes about 1.7 times the solar radius. At that point the radiative core extends to about 55% of the mass.

With further contraction, the luminosity increases slightly, and when the radius has contracted to 1.5 solar radii, the radiative core covers about 97% of the mass and 70% of the radius. At that point, the central temperature reaches about 9.6 million degrees. The last part of the calculated track, which corresponds to the points 1.2 $R_\odot$ and 1 $R_\odot$, has no physical significance since we did not consider the nuclear energy generation in our model calculations. By the time the sun contracts to that extent the central temperature has become high enough to take into account the energy generation by nuclear sources. The start of nuclear energy generation will change the route of the track and should bring the sun down into the initial main sequence, probably about as indicated by the dashed portion on the lower left of Fig. 4.

In our calculations, we assumed that the effective temperature of the star corresponds to the actual temperature at an optical depth 2/3. It can be argued that this is not a good assumption. In order to test the sensitivity of this choice, we reconstructed some of the models by taking this value as 0.5 and 1. The results for a partially convective model 2 $R_\odot$ and a fully convective model 20 $R_\odot$ corresponding to the optical depths $\tau = 0.5$, 2/3, and 1 are summarized in Table VI. An inspection of these results indicates that the differences due to this choice can be considered as insignificant.

Prandtl's mixing-length theory in the form given by E. Vitense (1958) has been used in treating the convection in spite of some severe defects in representing the convective heat fluxes near the surface layers (Spiegel, 1962; Simoda, 1961). The mixing length used here is the vertical distance that a moving element travels before it dissolves. It is usually taken as a constant multiple of the pressure scale height. There are still great uncertainties about the appropriate choice of this constant. Therefore, it has been customary to choose this ratio as a disposable parameter. We constructed most of our models by taking this parameter as unity. In order to see the influence of different values for the ratio of the mixing length to the pressure scale height, $\alpha = l/H$; we constructed models 2 $R_\odot$ and 20 $R_\odot$, also using the values 0.5, 2, and 3 for α. The results are summarized in Table VII. Figures 5 and 6 show the change of luminosity and effective temperature. The increase in α results in an increase in the luminosity of the star. The relative increase in luminosity is slightly greater in 20 $R_\odot$ which is a fully convective model. These results have special importance in the sense that the luminosity of protosun might be higher than the calculated one, if for α a more realistic value turns out to be larger than one.

With a larger ratio of the mixing length

TABLE VI

MODELS WITH EFFECTIVE TEMPERATURE AT DIFFERENT OPTICAL DEPTHS

$R/R\odot$	τ	T_e	$\rho_{surface}$	L	J	T_c	ρ_c
2	0.5000	4528	2.507×10^{-7}	5.792×10^{33}	2.118	4.203×10^{6}	1.314
2	0.6666	4550	2.915×10^{-7}	5.903×10^{33}	2.120	4.206×10^{6}	1.303
2	1.0000	4596	3.556×10^{-7}	6.145×10^{33}	2.118	4.218×10^{6}	1.303
20	0.5000	3926	3.120×10^{-8}	3.272×10^{35}	2.020	4.760×10^{5}	1.625×10^{-3}
20	0.6666	3941	3.638×10^{-8}	3.323×10^{35}	2.015	4.758×10^{5}	1.606×10^{-3}
20	1.0000	3971	4.486×10^{-8}	3.425×10^{35}	2.022	4.754×10^{5}	1.619×10^{-3}

TABLE VII

MODELS WITH DIFFERENT MIXING LENGTH ASSUMPTIONS

$R/R_\odot$	l/H	T_e	$\rho_{surface}$	L	T_c	ρ	T (conv)	(r/R) (conv)	(M_r/M) (conv)	$L/L_\odot$
2	0.5	4091	4.397×10^{-7}	3.858×10^{33}	4.140×10^{6}	1.452	3.02×10^{6}	0.42	0.25	1.02
2	1	4550	2.915×10^{-7}	5.903×10^{33}	4.206×10^{6}	1.303	3.31×10^{6}	0.33	0.15	1.56
2	2	5119	1.915×10^{-7}	9.450×10^{33}	4.347×10^{6}	1.239	3.78×10^{6}	0.23	0.07	2.50
2	3	5381	1.555×10^{-7}	1.156×10^{34}	4.331×10^{6}	1.239	4.11×10^{6}	0.11	0.01	3.06
20	0.5	3355	6.722×10^{-8}	1.745×10^{35}	4.718×10^{5}	1.578×10^{-3}	—	—	—	46.164
20	1	3941	3.638×10^{-8}	3.323×10^{35}	4.758×10^{5}	1.606×10^{-3}	—	—	—	87.91
20	2	4583	1.990×10^{-8}	6.077×10^{35}	4.790×10^{5}	1.659×10^{-3}	—	—	—	160.77
20	3	4970	1.480×10^{-8}	8.410×10^{35}	4.807×10^{5}	1.668×10^{-3}	—	—	—	222.48

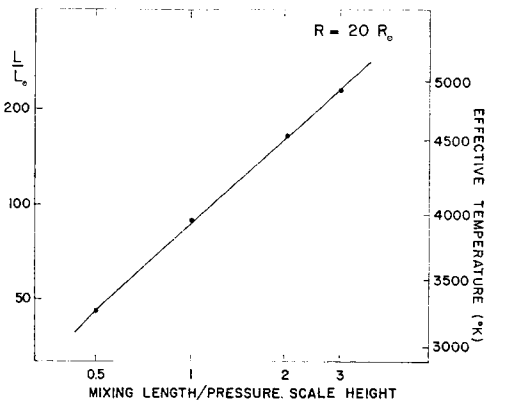

FIG. 5. The relation between luminosity and mixing length for a solar model with 20 times the present radius.

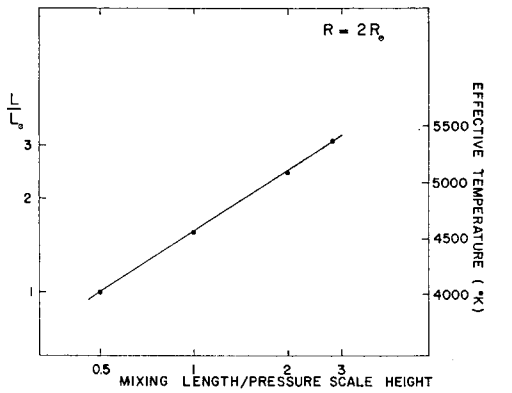

FIG. 6. The relation between luminosity and mixing length for a solar model with 2 times the present radius.

to the pressure scale height causing an increase in luminosity, also there is an accompanying extension of the convection zone towards the center of the star. In accordance with this, the temperature at the bottom of the convective zone increases, and reaches about 4.1×10^6 °K, for the model 2 $R_\odot$. The radiative core covers only 1% of the mass with the value $\alpha = 3$ while it is about 15% of the mass with $\alpha = 1$. These results are shown in Fig. 7.

Convection sets in at the optical depths of $\tau = 3.19$, 3.25, 2.05, and 1.94 for $\tau = 0.5$, 1, 2, and 3, respectively for 2 $R_\odot$.

In the transition regions where the density and the specific heat are low, the superadiative gradient $(\nabla - \nabla')$ and con-

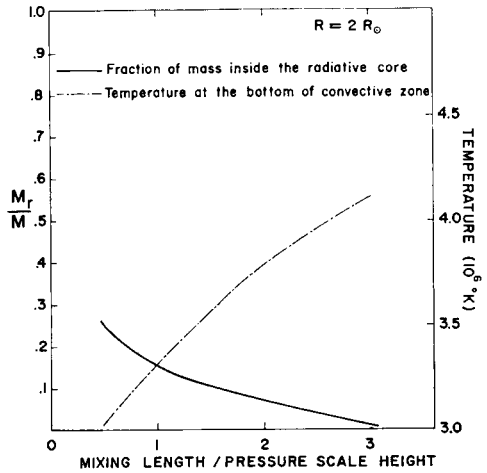

FIG. 7. Densities at the bottom of the outer convective zone in the solar model with twice the present radius, as a function of the assumed mixing length.

vective velocity $\bar{v}$ show a sudden increase in order to carry the required amount of flux. In Fig. 8 we have plotted the average convective velocity $\bar{v}$ versus log P for

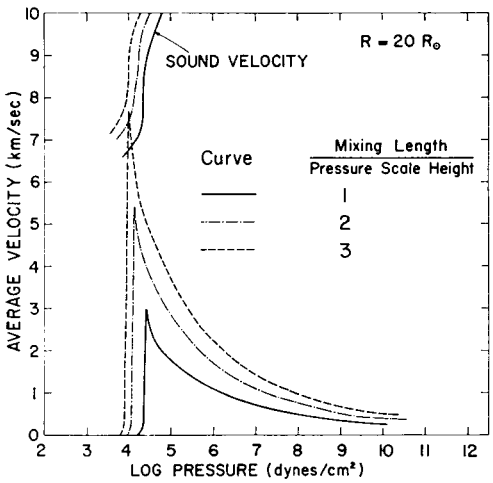

FIG. 8. The average velocity of the turbulent elements in the outer convective zone for a solar model of 20 times the present radius, shown for three assumptions concerning the mixing length. Also shown are the sound velocities at various points of the transition layers in the different models. The peak in the velocity curve is not realistically determined because the peak structure is narrow compared to the mixing length.

20 $R_\odot$. The increase in the ratio of mixing length to pressure scale height results in higher convective velocities; the convective velocity approaches that of sound and might initiate shock-wave phenomena if a large value of the ratio α should be the correct one.

We have also investigated the effect of using the density scale height as a measure of the mixing length. The procedure here is somewhat complicated by the fact that the models so far described have a density inversion immediately below the transition region in the photosphere where convection begins. This arises from the effects of an increasing opacity with depth and the corresponding steepening of the temperature gradient necessary to carry the radiative flux in the region before convection becomes efficient. To avoid these complications we took as the mixing length in the transition zone the actual distance required for the density to increase by a factor e below the point where convection commences. At greater depths the local density scale height was used.

With these changes the density inversion nearly disappeared. A model with radius 2 $R_\odot$ had a luminosity corresponding to a choice $\alpha = 1.4$ for the pressure scale height. A model with radius 20 $R_\odot$ had a luminosity corresponding to a choice $\alpha = 1.8$. These results are consistent with some calculations for a solar model carried out by Norman Baker (private communication).

The contraction time t for contraction between radii R_1 and R_2, can be found by the relation

$$t = \int_{R_1}^{R_2} \frac{d[E_{Gra} - (E_{Ther} + E_{ion} + E_{disso})]dR}{LdR}.$$

This integration has been carried out graphically. The luminosity and radius versus time have been plotted in Fig. 9, and also indicated in Fig. 4. It can be seen that the sun evolves very rapidly away from the threshold of stability. When it ceases to become fully convective its age is about half a million years; the time required to contract from 57 $R_\odot$ to 1.7 $R_\odot$, the radius corresponding about the minimum luminosity, is about one million years.

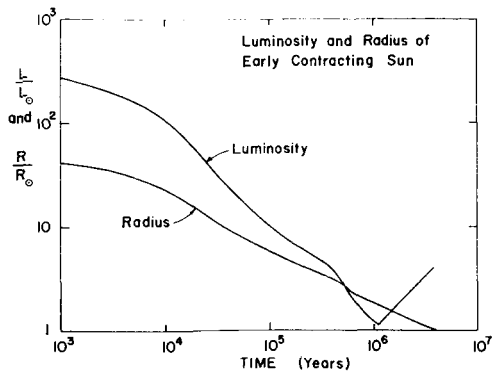

FIG. 9. The behavior of the luminosity and radius of the sun as a function of time beyond the threshold of stability.

The sun reaches approximately its present position near the main sequence in about 2×10^6 years.

These times are much shorter than the earlier estimates of the age of the sun at the end of its stage of Helmholz-Kelvin contraction.

In the calculation of these results, no energy generation due to the deuterium burning has been included. Let us consider when the deuterium burning would occur as the primitive sun contracts.

The energy generation rate for deuterium burning is given by

$$\epsilon = 4.3 \times 10^{23} \frac{x_H x_D \rho}{T_6^{2/3}} \exp\left(-\frac{37.2}{T_6^{1/3}}\right) \text{ erg/gm sec}$$

where x_H and x_D are the fractional hydrogen and deuterium abundances by mass, and T_6 is the temperature in unit of 10^6 °K. If the primitive sun had the terrestrial ratio of deuterium to hydrogen, this deuterium would be destroyed by thermonuclear reactions when the central temperature reaches about 800,000 °K. When the sun contracts to 10 solar radii, the energy generation by deuterium burning is equal to 1.03×10^{35} erg/sec. At this radius its luminosity is 28 times its present value. The contraction would halt at this point while the deuterium is destroyed. Since the sun is fully convective, the material would be well mixed inside the sun and the destruction of deuterium would go on throughout the sun. This deuterium burning stage of the early solar evolution would add about 3×10^5 years to the contraction age indicated in Fig. 9.

We should also give some consideration to the present abundance of lithium in the sun. This abundance is much smaller, relative to that of similar elements such as sodium or potassium, than is found for the earth and meteorites. Thermonuclear reactions with hydrogen above 4,000,000 °K rapidly destroy lithium. But we are determining the abundance of lithium in its surface layers. In order to find whether lithium in the surface layers should have been depleted by thermonuclear reactions, we must find the highest temperature which the convection zone attains at the bottom so that the material can be subjected to these temperatures by convective motion.

We can estimate how much lithium would have been destroyed during the contraction phase of the sun. Lithium contains two stable isotopes, Li^6 and Li^7. The reaction rate for Li^6 (p, α) He^3 reaction per nucleus per second is

$$\frac{P}{\rho x_H} = \frac{5.96 \times 10^{12}}{T_6^{2/3}} \exp\left(-84.149/T_6^{1/3}\right)$$

The similar reaction rate for Li^7 (p, α) He^4 is

$$\frac{P}{\rho x_H} = \frac{1.20 \times 10^{11}}{T_6^{2/3}} \exp\left(-84.731/T_6^{1/3}\right)$$

If we assume that the mixing is sufficiently rapid to keep the material homogeneous in the convective zone, then the relative number of lithium nuclei which have been destroyed in the convective zone can be obtained by integrating the reaction rates throughout the convection zone and dividing by the mass remaining inside the convective zone. For the fully convective model the surface material is well mixed with the center material, but the central temperatures have not risen above the critical value for the lithium thermonuclear reactions. When the sun contracts to 3 $R_\odot$, the central temperature is high enough to consider the thermonuclear reactions with hydrogen. With further contraction the temperature at the bottom of the

outer convective zone reaches the values listed in Table IV. These temperatures are sufficiently high to deplete the Li^6 by a substantial factor (3.24), but the depletion of Li^7 is insignificant (1.4%). In Fig. 10 is shown the rate of lithium burning versus time.

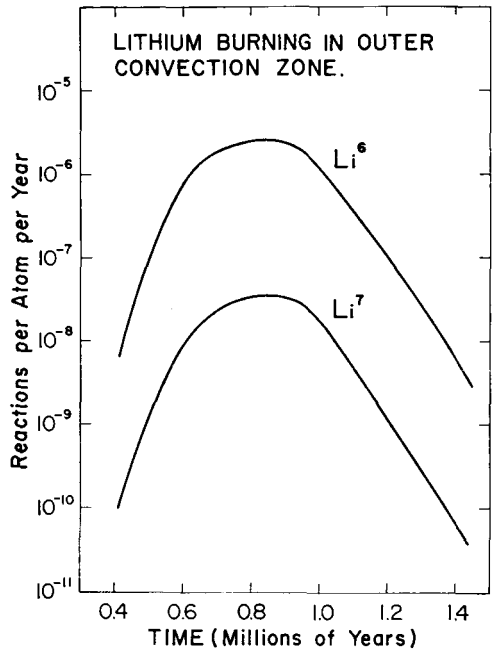

FIG. 10. The rate of lithium burning averaged throughout the outer convective zone for both isotopes of lithium, as a function of the evolutionary time of the solar models calculated with the mixing length assumed equal to the pressure scale height. The total depletion of the isotopes is obtained by integrating under these curves.

In Fig. 7, we showed the change of temperature at the bottom of the convective zone with different assumed values of the ratio of the mixing length to the pressure scale height. With a larger ratio of the mixing length to the pressure scale height the temperature at the bottom of the convective zone increases. Consequently the depletion of lithium would be more rapid. With $\alpha = 3$ for the 2 $R_\odot$ model, the outer convective zone reaches a temperature well over 4×10^6 °K. At these high temperatures the depletion of Li^7 would be appreciable (factor 2.2). If the primitive sun contains about the same amount of lithium, relative to sodium and potassium, as do the earth and the meteorites, then we could obtain about the observed amount of depletion of lithium in the surface layers of the sun by assuming a fairly large value for the ratio of mixing length of pressure scale height in constructing models of the contracting phases.

Some of these results are quite similar to those independently obtained by R. Weymann and E. Moore (to be published). The principal difference is that we find a greater probability of lithium burning than they did, probably because our interior opacities are greater than the ones they used, and hence our outer convection zones are somewhat deeper.

CONCLUSIONS

These calculations confirm Hayashi's prediction that the early contracting sun should be highly luminous and fully convective. We find that the sun contracts to approximately its main sequence position in 2 million years, but this figure may be still further reduced owing to the great uncertainties in the solar luminosity that we found associated with the theory of convection used. The maximum radius of the sun is 57 $R_\odot$; models with larger radii are unstable against gravitational collapse. If the terrestrial ratio of deuterium to hydrogen also existed in the early protosun, then deuterium burning adds 3×10^5 years to the solar contraction time. We find that the outer convection zone of the sun very probably became hot enough to cause a significant depletion of Li^6, but the depletion of Li^7 is highly uncertain and depends on the details of the convection theory. These conclusions have considerable relevance for theories of the origin of the solar system, since it appears that planets forming in a solar nebula formed with the sun must be subjected to a high temperature environment.

ACKNOWLEDGMENTS

The authors are grateful to Dr. A. N. Cox for providing the Los Alamos opacity code and for

consulting in regard to its use. They also wish to thank Mrs. Marilyn Golub and Mr. Leon Lefton for great assistance in carrying out the calculations that were performed on the Institute for Space Studies 7090 computer. One of us (D. Ezer) wishes to express appreciation to Dr. Robert Jastrow for the hospitality of the Institute for Space Studies during her tenure of a National Academy of Sciences–National Research Council Resident Research Associateship with the National Aeronautics and Space Administration.

REFERENCES

BROWNLEE, R. R., AND COX, A. N. (1961). *Sky and Tel.* **22**, 252.

CAMERON, A. G. W. (1959). *Astrophys. J.* **129**, 676.

CAMERON, A. G. W. (1962*a*). *Icarus* **1**, 13.

CAMERON, A. G. W. (1962*b*). *Sky and Tel.* **23**, 244.

COX, A. N. (1961). Preprint.

HAYASHI, C. (1961). *Publs. Astron. Soc. Japan* **13**, 450.

HENYEY, L. G., LE LEVIER, R., AND LEVEE, R. D. (1955). *Publs. Astron. Soc. Pacific* **67**, 154.

HOYLE, F. (1960). *Quart. J. Roy. Astron. Soc.* **1**, 28.

HOYLE, F., AND SCHWARZSCHILD, M. (1955). *Astrophys. J. Suppl.* **2**, 1.

SIMODA, M. (1961). *Publs. Astron. Soc. Japan* **13**, 424.

SPIEGEL, E. (1962). To be published.

VARDYA, M. S. (1961). *Astrophys. J.* **133**, 107.

VITENSE, E. B. (1951). *Z. Astrophys.* **28**, 81.

VITENSE, E. B. (1953). *Z. Astrophys.* **32**, 135.

VITENSE, E. B. (1958). *Z. Astrophys.* **46**, 108.